Int. J. Advance Soft Compu. Appl, Vol. 18, No. 1, March 2026
Print ISSN: 2710-1274, Online ISSN: 2074-8523

Modeling Anomalous Diffusion with the Fractional Brusselator

Maysoon Qousini[1], Waseem Al-Mashaleh[2]
[1]Department of Mathematics, Faculty of Science & Information Technology,
Al-Zaytoonah University of Jordan, Amman, Jordan
e-mail: m.qousini@zuj.edu.jo
[2]Department of Mathematics, Faculty of Science and Information Technology,
Al-Zaytoonah University of Jordan, Amman 11733, Jordan
e-mail: w.almashaleh@zuj.edu.jo

Abstract

This paper studies the fractional reaction-diffusion Brusselator model, which incorporates fractional-time derivatives to describe memory effects and anomalous diffusion in pattern formation. A fully discrete numerical scheme is developed using an L_1 approximation for the fractional derivative and a finite difference method for spatial discretization. Theoretical analysis proves the uniqueness, asymptotic stability, and convergence of the scheme. Numerical simulations demonstrate the emergence of stationary Turing patterns under appropriate conditions, validating the model's ability to capture complex spatiotemporal dynamics. The work provides a reliable computational framework for exploring fractional reaction-diffusion systems in two dimensions.

Keywords: *Fractional reaction-diffusion systems, Brusselator model, Turing patterns, L_1 approximation, Finite difference method, stability analysis.*

1 Introduction

RD systems provide a fundamental theoretical framework for understanding the spatiotemporal evolution of chemical and biological structures [1, 2]. These systems are driven by the intricate interplay between local reaction kinetics and spatial diffusion, a mechanism responsible for the emergence of ordered

Received: 6 October 2025; Accepted: 2 January 2026

structures from initially homogeneous states [3, 4]. Natural systems frequently exhibit such complex spatiotemporal patterns, ranging from animal coat markings to neuronal activity in the cerebral cortex [5, 6]. These structures typically arise under conditions far from thermodynamic equilibrium, where intrinsic instabilities drive the system from a uniform steady state toward a patterned configuration [7, 8]. In his seminal 1952 paper, Alan Turing demonstrated that the coupling between reaction kinetics and diffusion can lead to spontaneous symmetry breaking, a phenomenon now referred to as diffusion-driven instability or Turing bifurcation [9, 10]. Although diffusion is generally regarded as a homogenizing process, Turing showed that it can induce spatial order when interacting activator–inhibitor species possess sufficiently different diffusion rates [11, 12]. A general RD system involving two interacting species is governed by a set of coupled PDEs, in which the temporal evolution of the concentration vector is determined by nonlinear reaction terms and diffusion operators involving the Laplacian [13].

A paradigmatic example of such systems is the Brusselator, an autocatalytic theoretical model proposed by the Brussels school led by Ilya Prigogine [14, 15]. It represents a minimal framework capable of exhibiting Turing patterns while remaining chemically plausible. The model describes the interaction between an activator and an inhibitor species [16]. The dimensionless evolution equations governing the dynamics of the activator concentration $\mathfrak{u}$ and the inhibitor concentration $\mathfrak{v}$ in space and time are given by

$$\begin{cases} \dfrac{\partial \mathfrak{u}(x,y,t)}{\partial t} = D_{\mathfrak{u}}\nabla^2\mathfrak{u} + \mathfrak{a} - (\mathfrak{b}+1)\mathfrak{u} + \mathfrak{u}^2\mathfrak{v}, & (x,y,t) \in \Omega \times \mathbb{R}^+, \\ \dfrac{\partial \mathfrak{v}(x,y,t)}{\partial t} = D_{\mathfrak{v}}\nabla^2\mathfrak{v} + \mathfrak{b}\mathfrak{u} - \mathfrak{u}^2\mathfrak{v}, & (x,y,t) \in \Omega \times \mathbb{R}^+. \end{cases} \tag{1}$$

The system is characterized by two positive control parameters $\mathfrak{a}$ and $\mathfrak{b}$, which correspond to the externally maintained concentrations of input chemicals, along with the diffusion coefficients $D_{\mathfrak{u}}$ and $D_{\mathfrak{v}}$ for the activator and inhibitor, respectively [17]. The system admits a homogeneous steady state that may lose stability under appropriate conditions. Linear stability analysis reveals that a Turing instability, leading to the emergence of stationary spatial patterns, occurs when the inhibitor diffuses sufficiently faster than the activator, that is, when $D_{\mathfrak{v}} > D_{\mathfrak{u}}$. When this condition is satisfied and the bifurcation parameter $\mathfrak{b}$ exceeds a critical threshold, the system spontaneously transitions from a uniform state to stable, self-organized spatial structures [18, 19].

To investigate the dynamical behavior of the Brusselator model, including its stability properties and limit-cycle oscillations, numerical simulations can be constructed using Simulink [20, 21]. The underlying model is based on the dimensionless evolution equations presented above and focuses on the temporal evolution of $\mathfrak{u}$ and $\mathfrak{v}$. This is achieved either by neglecting diffusion, yielding a system of nonlinear ODEs, or by discretizing the diffusion terms for spatially

extended simulations [22, 23]. The core Simulink architecture consists of two coupled feedback loops corresponding to $\mathfrak{u}$ and $\mathfrak{v}$. Integrator blocks compute the state variables from their respective derivatives $\frac{d\mathfrak{u}}{dt}$ and $\frac{d\mathfrak{v}}{dt}$. The nonlinear autocatalytic term $\mathfrak{u}^2\mathfrak{v}$ is implemented using Product blocks and Math Function blocks. Gain blocks represent the parameters $\mathfrak{a}$ and $\mathfrak{b}$, as well as the linear reaction coefficients [24, 25]. For the coupled system, Sum blocks combine the reaction terms as follows:

- For the $\mathfrak{u}$ loop: constant production $\mathfrak{a}$, linear degradation $-(\mathfrak{b}+1)\mathfrak{u}$, and autocatalytic production $\mathfrak{u}^2\mathfrak{v}$.
- For the $\mathfrak{v}$ loop: production $\mathfrak{b}\mathfrak{u}$ and consumption $-\mathfrak{u}^2\mathfrak{v}$.

Scopes and phase-plane visualization tools are connected to the integrator outputs to monitor time-series trajectories and phase-space attractors [26, 27]. This configuration enables direct observation of the transition from a stable fixed point to a limit cycle as the parameter $\mathfrak{b}$ crosses the critical Hopf bifurcation threshold, given for the homogeneous system by $\mathfrak{b}_c = 1 + \mathfrak{a}^2$. Despite the extensive study of the classical Brusselator model, many natural and engineered systems exhibit memory effects and anomalous transport phenomena that cannot be adequately captured using integer-order derivatives [28]. To address this limitation, we extend the classical framework by incorporating FO time derivatives of Caputo type into the Brusselator equations [29]. This FO formulation naturally accounts for memory and hereditary effects and provides a more realistic description of pattern formation in viscoelastic media, biological tissues, and other complex systems where diffusion deviates from Fickian behavior [30, 31].

The primary contribution of this work is the development of a fully discrete numerical scheme that combines the L_1 approximation for the Caputo derivative with an FDM discretization of the spatial Laplacian. The proposed scheme is computationally efficient and is rigorously analyzed in terms of uniqueness, asymptotic stability, and convergence. Under mild conditions on the discretization parameters, we establish that the numerical solution converges to the exact solution with order $O((\Delta t)^{2-\alpha} + h^2)$, where $\alpha \in (0, 1]$ denotes the fractional order. By introducing FO dynamics into the Brusselator model, we are able to investigate anomalous diffusion regimes, such as subdiffusion, which are frequently observed in biological pattern formation processes. This approach bridges the gap between theoretical modeling and experimental observations by providing a flexible framework capable of capturing non-Markovian dynamics. Although Turing's theory of morphogenesis and the classical Brusselator model are well established, the majority of existing studies assume normal diffusion and memoryless kinetics. In contrast, fractional calculus has emerged as a powerful mathematical framework for modeling systems with memory

and nonlocal effects. Nevertheless, its application to pattern-forming RD systems remains relatively limited, particularly with respect to rigorous numerical analysis. This paper seeks to address this gap by:

1. Formulating an FO Brusselator model with Caputo time derivatives;
2. Developing a novel numerical scheme with proven stability and convergence properties;
3. Demonstrating, through numerical simulations, that the FO model retains the ability to generate Turing patterns.

By extending the Brusselator model to the FO setting and providing a reliable computational methodology, this work enhances our understanding of complex spatiotemporal phenomena in biological, chemical, and material systems where memory effects and anomalous transport play a significant role. The remainder of this paper is organized as follows. Section 2 introduces the FO Brusselator model and its discretization using the Method of Lines, the L_1 approximation, and FDM. Section 3 presents the stability and convergence analysis of the proposed numerical scheme. Section 4 reports numerical experiments illustrating Turing pattern formation. Finally, Section 5 concludes the paper and outlines directions for future research.

2 Model Description

To investigate the spatiotemporal evolution of the system numerically, we transform the continuous PDE model into a system of ODEs using the Method of Lines (MOL) [32, 33]. This approach consists of discretizing the spatial derivatives while retaining the time variable in continuous form, thereby yielding a system that is amenable to standard ODE solvers or implementation via Simulink integration blocks [34, 35]. We consider a two-dimensional square domain $\Omega = [0, L] \times [0, L]$, which is discretized into a uniform grid of $N \times N$ points. The spatial step size is defined by $h = \Delta x = \Delta y = \frac{L}{N-1}$. The grid points are denoted by (x_i, y_j), where $i, j = 1, \ldots, N$. The nodal approximations of the activator and inhibitor concentrations are given by

$$\mathfrak{u}_{i,j}(t) \approx \mathfrak{u}(x_i, y_j, t), \qquad \mathfrak{v}_{i,j}(t) \approx \mathfrak{v}(x_i, y_j, t). \tag{2}$$

The Laplacian operator ∇^2 in two spatial dimensions is approximated using the standard five-point central difference stencil. For a generic grid function U, the discrete Laplacian $\Delta_h U_{i,j}$ is defined as

$$\nabla^2 U_{i,j} \approx \Delta_h U_{i,j} = \frac{U_{i+1,j} + U_{i-1,j} + U_{i,j+1} + U_{i,j-1} - 4U_{i,j}}{h^2}. \tag{3}$$

Substituting this approximation into the Brusselator equations yields the following semi-discrete system of ODEs for each interior grid point (i, j), with $2 \leq i, j \leq N-1$:

$$\begin{cases} \dfrac{d\mathfrak{u}_{i,j}(t)}{dt} = \dfrac{D_{\mathfrak{u}}}{h^2}\Delta_h \mathfrak{u}_{i,j} + \mathfrak{a} - (\mathfrak{b}+1)\mathfrak{u}_{i,j} + \mathfrak{u}_{i,j}^2\mathfrak{v}_{i,j}, \\ \dfrac{d\mathfrak{v}_{i,j}(t)}{dt} = \dfrac{D_{\mathfrak{v}}}{h^2}\Delta_h \mathfrak{v}_{i,j} + \mathfrak{b}\mathfrak{u}_{i,j} - \mathfrak{u}_{i,j}^2\mathfrak{v}_{i,j}. \end{cases} \tag{4}$$

Zero-flux (Neumann) boundary conditions are imposed to ensure mass conservation within the domain, implying that no chemical species enter or leave Ω. In the discrete setting, these conditions are enforced via reflection at the boundaries:

$$\mathfrak{u}_{0,j} = \mathfrak{u}_{2,j}, \quad \mathfrak{u}_{N+1,j} = \mathfrak{u}_{N-1,j}, \quad \mathfrak{v}_{0,j} = \mathfrak{v}_{2,j}, \quad \mathfrak{v}_{N+1,j} = \mathfrak{v}_{N-1,j},$$

with analogous relations in the y-direction. This treatment modifies the Laplacian stencil at boundary and corner nodes. The resulting semi-discrete formulation reduces the original RD system to a coupled system of ODEs, which can be integrated in time to simulate the emergence of Turing patterns. To account for memory effects, we generalize the model by replacing the first-order time derivatives with Caputo FO derivatives of order α, where $0 < \alpha \leq 1$. The resulting semi-discrete FO-RD system is given by

$$\begin{cases} {}^{C}D_t^{\alpha}\mathfrak{u}_{i,j}(t) = \dfrac{D_{\mathfrak{u}}}{h^2}\Delta_h \mathfrak{u}_{i,j} + \mathfrak{a} - (\mathfrak{b}+1)\mathfrak{u}_{i,j} + \mathfrak{u}_{i,j}^2\mathfrak{v}_{i,j}, \\ {}^{C}D_t^{\alpha}\mathfrak{v}_{i,j}(t) = \dfrac{D_{\mathfrak{v}}}{h^2}\Delta_h \mathfrak{v}_{i,j} + \mathfrak{b}\mathfrak{u}_{i,j} - \mathfrak{u}_{i,j}^2\mathfrak{v}_{i,j}. \end{cases} \tag{5}$$

Here, ${}^{C}D_t^{\alpha}$ denotes the Caputo fractional derivative, as defined in [36] by

$${}^{C}D_t^{\alpha} f(t) = \frac{1}{\Gamma(1-\alpha)} \int_0^t (t-\tau)^{-\alpha} f'(\tau)\, d\tau. \tag{6}$$

To discretize the FO time derivative, we employ the L_1 FDM. Let Δt denote the time step size and $t_n = n\Delta t$ for $n = 0, 1, \ldots, M$, where $T = M\Delta t$ is the final simulation time. The numerical approximations at time t_n are denoted by $\mathfrak{u}_{i,j}^n$ and $\mathfrak{v}_{i,j}^n$. The Caputo derivative at $t = t_n$ is approximated in [37] as

$${}^{C}D_t^{\alpha}\mathfrak{u}_{i,j}(t_n) \approx \frac{(\Delta t)^{-\alpha}}{\Gamma(2-\alpha)} \sum_{k=0}^{n-1} b_k \left(\mathfrak{u}_{i,j}^{n-k} - \mathfrak{u}_{i,j}^{n-k-1}\right), \tag{7}$$

where the weights b_k are defined by

$$b_k = (k+1)^{1-\alpha} - k^{1-\alpha}, \qquad k = 0, 1, \ldots, n-1. \tag{8}$$

Substituting the L_1 approximation into the FO system yields the fully discrete scheme

$$\begin{cases} \dfrac{(\Delta t)^{-\alpha}}{\Gamma(2-\alpha)} \displaystyle\sum_{k=0}^{n-1} b_k \left(\mathfrak{u}_{i,j}^{n-k} - \mathfrak{u}_{i,j}^{n-k-1} \right) = \dfrac{D_{\mathfrak{u}}}{h^2} \Delta_h \mathfrak{u}_{i,j}^{n-1} + \mathfrak{a} - (\mathfrak{b}+1)\mathfrak{u}_{i,j}^{n-1} + (\mathfrak{u}_{i,j}^{n-1})^2 \mathfrak{v}_{i,j}^{n-1}, \\ \dfrac{(\Delta t)^{-\alpha}}{\Gamma(2-\alpha)} \displaystyle\sum_{k=0}^{n-1} b_k \left(\mathfrak{v}_{i,j}^{n-k} - \mathfrak{v}_{i,j}^{n-k-1} \right) = \dfrac{D_{\mathfrak{v}}}{h^2} \Delta_h \mathfrak{v}_{i,j}^{n-1} + \mathfrak{b}\mathfrak{u}_{i,j}^{n-1} - (\mathfrak{u}_{i,j}^{n-1})^2 \mathfrak{v}_{i,j}^{n-1}. \end{cases} \tag{9}$$

Introducing the backward difference operator

$$\nabla \mathfrak{u}_{i,j}^{n} = \mathfrak{u}_{i,j}^{n} - \mathfrak{u}_{i,j}^{n-1}, \qquad \nabla \mathfrak{v}_{i,j}^{n} = \mathfrak{v}_{i,j}^{n} - \mathfrak{v}_{i,j}^{n-1},$$

the scheme can be written compactly as

$$\begin{cases} \nabla \mathfrak{u}_{i,j}^{n} = - \displaystyle\sum_{k=1}^{n-1} b_k \nabla \mathfrak{u}_{i,j}^{n-k} + \dfrac{(\Delta t)^{\alpha}}{\Gamma(2-\alpha)} \left[\dfrac{D_{\mathfrak{u}}}{h^2} \Delta_h \mathfrak{u}_{i,j}^{n-1} + \mathfrak{a} - (\mathfrak{b}+1)\mathfrak{u}_{i,j}^{n-1} + (\mathfrak{u}_{i,j}^{n-1})^2 \mathfrak{v}_{i,j}^{n-1} \right], \\ \nabla \mathfrak{v}_{i,j}^{n} = - \displaystyle\sum_{k=1}^{n-1} b_k \nabla \mathfrak{v}_{i,j}^{n-k} + \dfrac{(\Delta t)^{\alpha}}{\Gamma(2-\alpha)} \left[\dfrac{D_{\mathfrak{v}}}{h^2} \Delta_h \mathfrak{v}_{i,j}^{n-1} + \mathfrak{b}\mathfrak{u}_{i,j}^{n-1} - (\mathfrak{u}_{i,j}^{n-1})^2 \mathfrak{v}_{i,j}^{n-1} \right]. \end{cases} \tag{10}$$

This fully discrete scheme enables the iterative computation of the concentrations $\mathfrak{u}$ and $\mathfrak{v}$ at each grid point for time levels $n = 1, 2, \ldots, M$, given appropriate initial conditions at $n = 0$ are prescribed as

$$\mathfrak{u}_{i,j}^{0} = \mathfrak{u}_0(x_i, y_j), \qquad \mathfrak{v}_{i,j}^{0} = \mathfrak{v}_0(x_i, y_j), \quad 1 \le i, j \le N, \tag{11}$$

where $\mathfrak{u}_0(x, y)$ and $\mathfrak{v}_0(x, y)$ are given sufficiently smooth functions defined on Ω.

3 Stability Analysis

Having derived the fully discrete numerical scheme (10) for the FO-RD system (5), we now proceed to analyze its stability properties. Stability analysis is crucial to ensure that the numerical solution remains bounded and converges to the exact solution as the discretization parameters are refined. In the following, we establish several theoretical results regarding the scheme's uniqueness, stability, and convergence. We begin by proving that the numerical scheme admits a unique solution under a condition on the discretization parameters (Theorem 1). Next, we demonstrate the asymptotic stability of the scheme (Theorem 2). Then, we derive bounds for the local truncation errors (Lemma 1), which are subsequently used to prove the convergence of the scheme (Theorem 3).

Theorem 1. *The numerical scheme* (10) *approximating the FO-RD system admits a unique solution* $U = (\mathfrak{u}^n, \mathfrak{v}^n)$ *in the Banach space* $\mathcal{B}$ *provided that the contraction coefficient* Λ *satisfies the following condition:*

$$\Lambda = 2T^{1-\alpha}(\Delta t)^{\alpha-1} + \frac{4(\Delta t)^\alpha \max(D_\mathfrak{u}, D_\mathfrak{v})}{\Gamma(2-\alpha)h^4} + \frac{2(\Delta t)^\alpha L}{\Gamma(2-\alpha)} < 1. \tag{12}$$

Proof. Let Ω_h be the discrete spatial domain. We define $\mathcal{S}_h$ as the space of discrete grid functions $U = \{U_{i,j}^n\}$ defined on $\Omega_h \times \{t_0, t_1, \ldots, t_M\}$. We equip $\mathcal{S}_h$ with the supremum norm (infinity norm):

$$\|U\|_\infty = \max_{0\le n\le M} \max_{i,j} |U_{i,j}^n|. \tag{13}$$

Let $\mathcal{B} = \mathcal{S}_h \times \mathcal{S}_h$ be the product space for the vector of concentrations $(\mathfrak{u}, \mathfrak{v})$, equipped with the norm

$$\|(\mathfrak{u}, \mathfrak{v})\|_\infty = \max(\|\mathfrak{u}\|_\infty, \|\mathfrak{v}\|_\infty). \tag{14}$$

Since the domain is finite, $\mathcal{B}$ is a Banach space [38]. The system (10) is derived from the L_1 approximation of the Caputo derivative. We define the operator $\mathcal{T} : \mathcal{B} \to \mathcal{B}$ by rearranging (10) to isolate the terms at time step n. Let $\mu = \frac{(\Delta t)^\alpha}{\Gamma(2-\alpha)}$. The components of $\mathcal{T}(\mathfrak{u}, \mathfrak{v})$ at step n are defined as:

$$\mathcal{T}_1(\mathfrak{u}, \mathfrak{v})_{i,j}^n = \mathfrak{u}_{i,j}^{n-1} - \sum_{k=1}^{n-1} b_k \nabla \mathfrak{u}_{i,j}^{n-k} + \mu \left[\frac{D_\mathfrak{u}}{h^2} \Delta_h \mathfrak{u}_{i,j}^{n-1} + \mathfrak{a} - (\mathfrak{b}+1)\mathfrak{u}_{i,j}^{n-1} + (\mathfrak{u}_{i,j}^{n-1})^2 \mathfrak{v}_{i,j}^{n-1} \right],$$
$$\mathcal{T}_2(\mathfrak{u}, \mathfrak{v})_{i,j}^n = \mathfrak{v}_{i,j}^{n-1} - \sum_{k=1}^{n-1} b_k \nabla \mathfrak{v}_{i,j}^{n-k} + \mu \left[\frac{D_\mathfrak{v}}{h^2} \Delta_h \mathfrak{v}_{i,j}^{n-1} + \mathfrak{b}\mathfrak{u}_{i,j}^{n-1} - (\mathfrak{u}_{i,j}^{n-1})^2 \mathfrak{v}_{i,j}^{n-1} \right].$$

Let

$$\begin{cases} f(\mathfrak{u}, \mathfrak{v}) = \mathfrak{a} - (\mathfrak{b}+1)\mathfrak{u} + \mathfrak{u}^2\mathfrak{v} \\ g(\mathfrak{u}, \mathfrak{v}) = \mathfrak{b}\mathfrak{u} - \mathfrak{u}^2\mathfrak{v}. \end{cases}$$

These functions are Lipschitz continuous with constant L for bounded arguments. The Jacobian matrix of the reaction terms is given by:

$$J(\mathfrak{u}, \mathfrak{v}) = \begin{pmatrix} \frac{\partial f}{\partial \mathfrak{u}} & \frac{\partial f}{\partial \mathfrak{v}} \\ \frac{\partial g}{\partial \mathfrak{u}} & \frac{\partial g}{\partial \mathfrak{v}} \end{pmatrix} = \begin{pmatrix} -(\mathfrak{b}+1) + 2\mathfrak{u}\mathfrak{v} & \mathfrak{u}^2 \\ \mathfrak{b} - 2\mathfrak{u}\mathfrak{v} & -\mathfrak{u}^2 \end{pmatrix}. \tag{15}$$

We assume the concentrations $\mathfrak{u}$ and $\mathfrak{v}$ are bounded within a compact domain $\mathcal{D} = [0, \mathfrak{u}_{\max}] \times [0, \mathfrak{v}_{\max}]$, which is physically consistent for RD systems. Let

$K = \max(\mathfrak{u}_{\max}, \mathfrak{v}_{\max})$. We can bound the magnitude of the partial derivatives as follows:

$$\left|\frac{\partial f}{\partial \mathfrak{u}}\right| = |-(\mathfrak{b}+1) + 2\mathfrak{u}\mathfrak{v}| \leq \mathfrak{b} + 1 + 2K^2, \quad \left|\frac{\partial f}{\partial \mathfrak{v}}\right| = |\mathfrak{u}^2| \leq K^2,$$
$$\left|\frac{\partial g}{\partial \mathfrak{u}}\right| = |\mathfrak{b} - 2\mathfrak{u}\mathfrak{v}| \leq \mathfrak{b} + 2K^2, \quad \left|\frac{\partial g}{\partial \mathfrak{v}}\right| = |-\mathfrak{u}^2| \leq K^2.$$

Since all partial derivatives are uniformly bounded on the compact domain $\mathcal{D}$, the functions f and g are Lipschitz continuous. The Lipschitz constant L is determined by the infinity norm (maximum row sum) of the Jacobian matrix on the domain $\mathcal{D}$. Using the bounds derived above:

$$\begin{aligned}\|J(\mathfrak{u},\mathfrak{v})\|_\infty &= \max\left(\left|\frac{\partial f}{\partial \mathfrak{u}}\right| + \left|\frac{\partial f}{\partial \mathfrak{v}}\right|, \left|\frac{\partial g}{\partial \mathfrak{u}}\right| + \left|\frac{\partial g}{\partial \mathfrak{v}}\right|\right) \\ &\leq \mathfrak{b} + 1 + 3K^2.\end{aligned}$$

Thus, we may choose $L = \mathfrak{b} + 1 + 3K^2$ to satisfy the Lipschitz condition. Taking the difference for the components:

$$\begin{aligned}|\mathcal{T}_1(\mathfrak{u},\mathfrak{v})^n_{i,j} - \mathcal{T}_1(\tilde{\mathfrak{u}},\tilde{\mathfrak{v}})^n_{i,j}| &\leq |\mathfrak{u}^{n-1}_{i,j} - \tilde{\mathfrak{u}}^{n-1}_{i,j}| + \sum_{k=1}^{n-1} |b_k||\nabla(\mathfrak{u}-\tilde{\mathfrak{u}})^{n-k}_{i,j}| \\ &\quad + \mu\left|\frac{D_{\mathfrak{u}}}{h^2}\Delta_h(\mathfrak{u}-\tilde{\mathfrak{u}})^{n-1}_{i,j}\right| + \mu|f(\mathfrak{u},\mathfrak{v}) - f(\tilde{\mathfrak{u}},\tilde{\mathfrak{v}})|, \\ |\mathcal{T}_2(\mathfrak{u},\mathfrak{v})^n_{i,j} - \mathcal{T}_2(\tilde{\mathfrak{u}},\tilde{\mathfrak{v}})^n_{i,j}| &\leq |\mathfrak{v}^{n-1}_{i,j} - \tilde{\mathfrak{v}}^{n-1}_{i,j}| + \sum_{k=1}^{n-1} |b_k||\nabla(\mathfrak{v}-\tilde{\mathfrak{v}})^{n-k}_{i,j}| \\ &\quad + \mu\left|\frac{D_{\mathfrak{v}}}{h^2}\Delta_h(\mathfrak{v}-\tilde{\mathfrak{v}})^{n-1}_{i,j}\right| + \mu|g(\mathfrak{u},\mathfrak{v}) - g(\tilde{\mathfrak{u}},\tilde{\mathfrak{v}})|.\end{aligned} \tag{16}$$

We proceed by estimating the norms of the difference terms. Using the definition of the supremum norm, we have:

$$|\mathfrak{u}^{n-1}_{i,j} - \tilde{\mathfrak{u}}^{n-1}_{i,j}| \leq \max_{0\leq k\leq M}\max_{p,q}|\mathfrak{u}^k_{p,q} - \tilde{\mathfrak{u}}^k_{p,q}| = \|\mathfrak{u}-\tilde{\mathfrak{u}}\|_\infty.$$

Next,

$$\begin{aligned}\left|\Delta_h(\mathfrak{u}-\tilde{\mathfrak{u}})^{n-1}_{i,j}\right| &= \left|\frac{(\mathfrak{u}-\tilde{\mathfrak{u}})^{n-1}_{i+1,j} - 2(\mathfrak{u}-\tilde{\mathfrak{u}})^{n-1}_{i,j} + (\mathfrak{u}-\tilde{\mathfrak{u}})^{n-1}_{i-1,j}}{h^2}\right| \\ &\leq \frac{1}{h^2}\left(|(\mathfrak{u}-\tilde{\mathfrak{u}})^{n-1}_{i+1,j}| + 2|(\mathfrak{u}-\tilde{\mathfrak{u}})^{n-1}_{i,j}| + |(\mathfrak{u}-\tilde{\mathfrak{u}})^{n-1}_{i-1,j}|\right) \\ &\leq \frac{1}{h^2}\left(\|\mathfrak{u}-\tilde{\mathfrak{u}}\|_\infty + 2\|\mathfrak{u}-\tilde{\mathfrak{u}}\|_\infty + \|\mathfrak{u}-\tilde{\mathfrak{u}}\|_\infty\right) \\ &= \frac{4}{h^2}\|\mathfrak{u}-\tilde{\mathfrak{u}}\|_\infty.\end{aligned}$$

Applying the triangle inequality and the definition of the supremum norm:

$$|\nabla(\mathfrak{u}-\tilde{\mathfrak{u}})_{i,j}^{n-k}| \leq |(\mathfrak{u}-\tilde{\mathfrak{u}})_{i,j}^{n-k}| + |(\mathfrak{u}-\tilde{\mathfrak{u}})_{i,j}^{n-k-1}| \leq 2\|\mathfrak{u}-\tilde{\mathfrak{u}}\|_\infty. \tag{17}$$

Substituting the bounds for the Laplacian and the nonlinear functions into the component differences, we have for the first component:

$$\begin{aligned}
|\mathcal{T}_1(\mathfrak{u},\mathfrak{v})_{i,j}^n - \mathcal{T}_1(\tilde{\mathfrak{u}},\tilde{\mathfrak{v}})_{i,j}^n| &\leq \left(1+2\sum_{k=1}^{n-1} b_k + \frac{4\mu D_\mathfrak{u}}{h^4} + \mu L\right)\|\mathfrak{u}-\tilde{\mathfrak{u}}\|_\infty + \mu L\|\mathfrak{v}-\tilde{\mathfrak{v}}\|_\infty,\\
|\mathcal{T}_2(\mathfrak{u},\mathfrak{v})_{i,j}^n - \mathcal{T}_2(\tilde{\mathfrak{u}},\tilde{\mathfrak{v}})_{i,j}^n| &\leq \mu L\|\mathfrak{u}-\tilde{\mathfrak{u}}\|_\infty + \left(1+2\sum_{k=1}^{n-1} b_k + \frac{4\mu D_\mathfrak{v}}{h^4} + \mu L\right)\|\mathfrak{v}-\tilde{\mathfrak{v}}\|_\infty,
\end{aligned} \tag{18}$$

Combining the estimates for both components and utilizing the definition of the norm on the product space $\mathcal{B}$, we obtain the following bound for the operator:

$$\begin{aligned}
\|\mathcal{T}(\mathfrak{u},\mathfrak{v}) - \mathcal{T}(\tilde{\mathfrak{u}},\tilde{\mathfrak{v}})\|_\infty &\leq \left(1+2\sum_{k=1}^{n-1} b_k + \frac{4\mu\max(D_\mathfrak{u},D_\mathfrak{v})}{h^4} + 2\mu L\right)\|(\mathfrak{u}-\tilde{\mathfrak{u}},\mathfrak{v}-\tilde{\mathfrak{v}})\|_\infty\\
&\leq \left(2n^{1-\alpha} + \frac{4\mu\max(D_\mathfrak{u},D_\mathfrak{v})}{h^4} + 2\mu L\right)\|(\mathfrak{u}-\tilde{\mathfrak{u}},\mathfrak{v}-\tilde{\mathfrak{v}})\|_\infty\\
&\leq \left(2T^{1-\alpha}(\Delta t)^{\alpha-1} + \frac{4(\Delta t)^\alpha\max(D_\mathfrak{u},D_\mathfrak{v})}{\Gamma(2-\alpha)h^4} + \frac{2(\Delta t)^\alpha L}{\Gamma(2-\alpha)}\right)\|(\mathfrak{u}-\tilde{\mathfrak{u}},\mathfrak{v}-\tilde{\mathfrak{v}})\|_\infty\\
&= \Lambda\|(\mathfrak{u}-\tilde{\mathfrak{u}},\mathfrak{v}-\tilde{\mathfrak{v}})\|_\infty.
\end{aligned} \tag{19}$$

Denote the coefficient on the right-hand side by Λ. For the mapping $\mathcal{T}$ to be a contraction, we require $\Lambda < 1$. This condition imposes a constraint on the time step Δt and the mesh size h. Assuming this condition is satisfied, the operator $\mathcal{T}$ is a contraction mapping on the Banach space $\mathcal{B}$. Therefore, by the Banach Fixed Point Theorem, there exists a unique fixed point for $\mathcal{T}$, which implies that the numerical solution to the system (10) exists and is unique.

□

Theorem 2. *The fully discrete numerical scheme* (10) *approximating the FO-RD system is asymptotically stable. Specifically, the error energy* E^n *satisfies* $\lim_{n\to\infty} E^n = 0$*, provided that the time step* Δt *and grid spacing* h *are chosen such that the condition* $0 < C < 1$ *holds, where* C *depends on the diffusion coefficients and reaction parameters.*

Proof. Subtracting the equations for the exact solution from the equations for the numerical solution, we obtain the error evolution equations. For the linear

diffusion part, substituting the error terms into (22) (neglecting the nonlinear terms for the sufficient stability condition of the linear operator):

$$\begin{aligned}
\nabla\varepsilon_{i,j}^{n} &= -\sum_{k=1}^{n-1} b_k \nabla\varepsilon_{i,j}^{n-k} + \frac{(\Delta t)^{\alpha}}{\Gamma(2-\alpha)} \frac{D_{\mathfrak{u}}}{h^2} \left[\frac{D_{\mathfrak{u}}}{h^2} \Delta_h \varepsilon_{i,j}^{n-1} - (\mathfrak{b}+1)\varepsilon_{i,j}^{n-1} + (\tilde{\mathfrak{u}}_{i,j}^{n-1})^2 \tilde{\mathfrak{v}}_{i,j}^{n-1} - (\mathfrak{u}_{i,j}^{n-1})^2 \mathfrak{v}_{i,j}^{n-1} \right], \\
\nabla\delta_{i,j}^{n} &= -\sum_{k=1}^{n-1} b_k \nabla\delta_{i,j}^{n-k} + \frac{(\Delta t)^{\alpha}}{\Gamma(2-\alpha)} \left[\frac{D_{\mathfrak{v}}}{h^2} \Delta_h \delta_{i,j}^{n-1} + \mathfrak{b}\varepsilon_{i,j}^{n-1} - (\tilde{\mathfrak{u}}_{i,j}^{n-1})^2 \tilde{\mathfrak{v}}_{i,j}^{n-1} + (\mathfrak{u}_{i,j}^{n-1})^2 \mathfrak{v}_{i,j}^{n-1} \right].
\end{aligned} \tag{20}$$

To analyze the stability using the Lyapunov method, we consider the linearized form of the error system. We assume the nonlinear terms satisfy a Lipschitz condition or are negligible for the linear stability limit. Let us define the discrete Lyapunov energy function (the L_2-norm of the error) at time step n as

$$E^n = \sum_{i,j} |\varepsilon_{i,j}^n|^2 + \sum_{i,j} |\delta_{i,j}^n|^2. \tag{21}$$

We define the error terms as $\varepsilon_{i,j}^n = \tilde{\mathfrak{u}}_{i,j}^n - \mathfrak{u}_{i,j}^n$ and $\delta_{i,j}^n = \tilde{\mathfrak{v}}_{i,j}^n - \mathfrak{v}_{i,j}^n$. We analyze the variation of the energy $\nabla E^n = E^n - E^{n-1}$. Using the algebraic identity $a^2 - b^2 \leq 2a(a-b)$, we obtain the initial bound:

$$\nabla E^n \leq \sum_{i,j} 2\,\varepsilon_{i,j}^n\,\nabla\varepsilon_{i,j}^n + \sum_{i,j} 2\,\delta_{i,j}^n\,\nabla\delta_{i,j}^n. \tag{22}$$

Substituting the error evolution equations (20) into the inequality above yields:

$$\begin{aligned}
\nabla E^n \leq \sum_{i,j} 2\,\varepsilon_{i,j}^n \Bigg[&-\sum_{k=1}^{n-1} b_k \nabla\varepsilon_{i,j}^{n-k} + \frac{(\Delta t)^{\alpha}}{\Gamma(2-\alpha)} \frac{D_{\mathfrak{u}}}{h^2} \Bigg(\frac{D_{\mathfrak{u}}}{h^2} \Delta_h \varepsilon_{i,j}^{n-1} - (\mathfrak{b}+1)\varepsilon_{i,j}^{n-1} \\
&+ (\tilde{\mathfrak{u}}_{i,j}^{n-1})^2 \tilde{\mathfrak{v}}_{i,j}^{n-1} - (\mathfrak{u}_{i,j}^{n-1})^2 \mathfrak{v}_{i,j}^{n-1} \Bigg) \Bigg] \\
+ \sum_{i,j} 2\,\delta_{i,j}^n \Bigg[&-\sum_{k=1}^{n-1} b_k \nabla\delta_{i,j}^{n-k} + \frac{(\Delta t)^{\alpha}}{\Gamma(2-\alpha)} \Bigg(\frac{D_{\mathfrak{v}}}{h^2} \Delta_h \delta_{i,j}^{n-1} + \mathfrak{b}\varepsilon_{i,j}^{n-1} \\
&- (\tilde{\mathfrak{u}}_{i,j}^{n-1})^2 \tilde{\mathfrak{v}}_{i,j}^{n-1} + (\mathfrak{u}_{i,j}^{n-1})^2 \mathfrak{v}_{i,j}^{n-1} \Bigg) \Bigg].
\end{aligned} \tag{23}$$

We now estimate the terms on the right-hand side. The diffusion term is bounded using the spectral properties of the discrete Laplacian, where the eigenvalues are bounded by $-\frac{4}{h^2}\sin^2(\frac{\pi}{2N})$. The nonlinear terms are estimated

using the Lipschitz condition with constant L:

$$\begin{aligned}\nabla E^n \leq \frac{2(\Delta t)^\alpha}{\Gamma(2-\alpha)} \sum_{i,j} \Bigg[& -\frac{4D_{\mathfrak{u}}}{h^2} \sin^2\Big(\frac{\pi}{2N}\Big) |\varepsilon_{i,j}^{n-1}|^2 - (\mathfrak{b}+1)|\varepsilon_{i,j}^{n-1}|^2 \\ & + L|\varepsilon_{i,j}^{n-1}|\Big(|\varepsilon_{i,j}^{n-1}| + |\delta_{i,j}^{n-1}|\Big)\Bigg] \\ & + \frac{2(\Delta t)^\alpha}{\Gamma(2-\alpha)} \sum_{i,j} \Bigg[-\frac{4D_{\mathfrak{v}}}{h^2} \sin^2\Big(\frac{\pi}{2N}\Big) |\delta_{i,j}^{n-1}|^2 + \mathfrak{b}|\varepsilon_{i,j}^{n-1}||\delta_{i,j}^{n-1}| \\ & + L|\delta_{i,j}^{n-1}|\Big(|\varepsilon_{i,j}^{n-1}| + |\delta_{i,j}^{n-1}|\Big)\Bigg]. \end{aligned} \tag{24}$$

Let $\lambda_{\mathfrak{u}} = \frac{4D_{\mathfrak{u}}}{h^2} \sin^2\left(\frac{\pi}{2N}\right)$ and $\lambda_{\mathfrak{v}} = \frac{4D_{\mathfrak{v}}}{h^2} \sin^2\left(\frac{\pi}{2N}\right)$. Grouping the coefficients of $|\varepsilon_{i,j}^{n-1}|^2$, $|\delta_{i,j}^{n-1}|^2$, and the cross terms results in:

$$\begin{aligned}\nabla E^n &\leq \frac{2(\Delta t)^\alpha}{\Gamma(2-\alpha)} \sum_{i,j} \Big[-(\lambda_{\mathfrak{u}} + \mathfrak{b} + 1 - L)|\varepsilon_{i,j}^{n-1}|^2 + L|\varepsilon_{i,j}^{n-1}||\delta_{i,j}^{n-1}|\Big] \\ &\quad + \frac{2(\Delta t)^\alpha}{\Gamma(2-\alpha)} \sum_{i,j} \Big[-(\lambda_{\mathfrak{v}} - L)|\delta_{i,j}^{n-1}|^2 + (\mathfrak{b} + L)|\varepsilon_{i,j}^{n-1}||\delta_{i,j}^{n-1}|\Big] \\ &\leq \frac{(\Delta t)^\alpha}{\Gamma(2-\alpha)} \sum_{i,j} \Big[-2(\lambda_{\mathfrak{u}} + \mathfrak{b} + 1 - L)|\varepsilon_{i,j}^{n-1}|^2 - 2(\lambda_{\mathfrak{v}} - L)|\delta_{i,j}^{n-1}|^2 \\ &\quad + (\mathfrak{b} + 2L)\Big(|\varepsilon_{i,j}^{n-1}|^2 + |\delta_{i,j}^{n-1}|^2\Big)\Big]. \end{aligned} \tag{25}$$

Finally, simplifying the expression further by determining the sufficient conditions for the coefficients to be negative definite, we obtain the final stability bound:

$$\nabla E^n \leq -C \sum_{i,j} \Big(|\varepsilon_{i,j}^{n-1}|^2 + |\delta_{i,j}^{n-1}|^2\Big) = -CE^{n-1}, \tag{26}$$

where the constant C is defined by the maximum of the coefficients derived in the previous step:

$$C = \frac{(\Delta t)^\alpha}{\Gamma(2-\alpha)} \max\left\{2\lambda_{\mathfrak{u}} + \mathfrak{b} + 2 - 4L,\ 2\lambda_{\mathfrak{v}} - \mathfrak{b} - 4L\right\} > 0.$$

From the inequality $\nabla E^n \leq -CE^{n-1}$, we have

$$E^n \leq (1-C)E^{n-1}.$$

Assuming the time step Δt and grid spacing h are chosen such that $0 < C < 1$, the energy satisfies $E^n < E^{n-1}$. By recursive application, we obtain $E^n \leq$

$(1-C)^n E^0$. Since E^0 is bounded (determined by the initial approximation errors), $\lim_{n\to\infty} E^n = 0$. This confirms that the error system is asymptotically stable. □

Lemma 1. *Suppose that the exact solution* $(\mathfrak{u}(x,y,t), \mathfrak{v}(x,y,t))$ *of the FO RD system is sufficiently smooth. The local truncation errors* $R^n_{\mathfrak{u},i,j}$ *and* $R^n_{\mathfrak{v},i,j}$ *of the fully discrete numerical scheme* (10) *satisfy the following inequalities, where* C_1 *and* C_2 *are positive constants independent of* Δt *and* h*:*

$$|R^n_{\mathfrak{u},i,j}| \le C_1\left((\Delta t)^{2-\alpha} + h^2\right), \quad |R^n_{\mathfrak{v},i,j}| \le C_2\left((\Delta t)^{2-\alpha} + h^2\right) \tag{27}$$

Proof. The truncation error $R^n_{\mathfrak{u},i,j}$ is defined as the difference between the continuous operator and the discrete operator applied to the exact solution:

$$R^n_{\mathfrak{u},i,j} = \left(\frac{\partial^\alpha \mathfrak{u}}{\partial t^\alpha} - L_t^\alpha \mathfrak{u}\right)^n_{i,j} - D_{\mathfrak{u}}\left(\Delta \mathfrak{u} - \Delta_h \mathfrak{u}\right)^n_{i,j}.$$

We analyze the temporal and spatial errors separately. The Caputo fractional derivative is defined as:

$$\frac{\partial^\alpha \mathfrak{u}}{\partial t^\alpha}(t_n) = \frac{1}{\Gamma(1-\alpha)} \sum_{k=0}^{n-1} \int_{t_k}^{t_{k+1}} \frac{\mathfrak{u}'(s)}{(t_n - s)^\alpha}\, ds. \tag{28}$$

The L_1 approximation replaces the derivative $\mathfrak{u}'(s)$ on the interval $[t_k, t_{k+1}]$ with the finite difference slope $\frac{\mathfrak{u}(t_{k+1})-\mathfrak{u}(t_k)}{\Delta t}$:

$$L_t^\alpha \mathfrak{u}(t_n) = \frac{1}{\Gamma(1-\alpha)} \sum_{k=0}^{n-1} \frac{\mathfrak{u}(t_{k+1}) - \mathfrak{u}(t_k)}{\Delta t} \int_{t_k}^{t_{k+1}} \frac{1}{(t_n - s)^\alpha}\, ds. \tag{29}$$

Subtracting the two expressions gives the error:

$$E_t = \frac{\partial^\alpha \mathfrak{u}}{\partial t^\alpha}(t_n) - L_t^\alpha \mathfrak{u}(t_n) = \frac{1}{\Gamma(1-\alpha)} \sum_{k=0}^{n-1} \int_{t_k}^{t_{k+1}} \frac{\mathfrak{u}'(s) - \frac{\mathfrak{u}(t_{k+1})-\mathfrak{u}(t_k)}{\Delta t}}{(t_n - s)^\alpha}\, ds. \tag{30}$$

Using Taylor's theorem with remainder, for any $s \in [t_k, t_{k+1}]$, the error in the derivative approximation is bounded by the second derivative:

$$\left|\mathfrak{u}'(s) - \frac{\mathfrak{u}(t_{k+1}) - \mathfrak{u}(t_k)}{\Delta t}\right| \le C_{\mathfrak{u}}(\Delta t) \max_{t\in[0,T]} |\mathfrak{u}''(t)|. \tag{31}$$

Substituting this bound into the integral:

$$\begin{aligned} |E_t| &\le \frac{C_{\mathfrak{u}}\Delta t}{\Gamma(1-\alpha)} \max|\mathfrak{u}''| \sum_{k=0}^{n-1} \int_{t_k}^{t_{k+1}} (t_n - s)^{-\alpha}\, ds \\ &= \frac{C_{\mathfrak{u}}\Delta t}{\Gamma(1-\alpha)} \max|\mathfrak{u}''| \sum_{k=0}^{n-1} \left[\frac{-(t_n - s)^{1-\alpha}}{1-\alpha}\right]_{t_k}^{t_{k+1}} \\ &= \frac{C_{\mathfrak{u}}\Delta t}{\Gamma(2-\alpha)} \max|\mathfrak{u}''| \sum_{k=0}^{n-1} \left((t_n - t_k)^{1-\alpha} - (t_n - t_{k+1})^{1-\alpha}\right). \end{aligned} \tag{32}$$

Noting that $t_n - t_k = (n-k)\Delta t$, the telescoping sum (or direct evaluation) simplifies. The largest term dominates, yielding an order of $(\Delta t)^{1-\alpha}$ multiplied by the outside Δt:

$$|E_t| \leq C_t(\Delta t)^{2-\alpha}.$$

We define the spatial truncation error $E_s = D_{\mathfrak{u}}(\Delta\mathfrak{u} - \Delta_h\mathfrak{u})$ at point (x_i, y_j). We consider the expansion in the x-direction (the y-direction is identical). Using the Taylor series expansion around x_i:

$$\begin{aligned}
\mathfrak{u}(x_{i+1}) &= \mathfrak{u}(x_i) + h\mathfrak{u}'_x(x_i) + \frac{h^2}{2!}\mathfrak{u}''_{xx}(x_i) + \frac{h^3}{3!}\mathfrak{u}'''_{xxx}(x_i) + \frac{h^4}{4!}\mathfrak{u}^{(4)}_{xxxx}(\xi_1),\\
\mathfrak{u}(x_{i-1}) &= \mathfrak{u}(x_i) - h\mathfrak{u}'_x(x_i) + \frac{h^2}{2!}\mathfrak{u}''_{xx}(x_i) - \frac{h^3}{3!}\mathfrak{u}'''_{xxx}(x_i) + \frac{h^4}{4!}\mathfrak{u}^{(4)}_{xxxx}(\xi_2).
\end{aligned}$$

Adding these two equations, the odd derivative terms cancel out:

$$\mathfrak{u}(x_{i+1}) + \mathfrak{u}(x_{i-1}) = 2\mathfrak{u}(x_i) + h^2\mathfrak{u}''_{xx}(x_i) + \frac{h^4}{24}\left(\mathfrak{u}^{(4)}_{xxxx}(\xi_1) + \mathfrak{u}^{(4)}_{xxxx}(\xi_2)\right).$$

Rearranging to solve for the second derivative $\mathfrak{u}''_{xx}$ (which is part of the Laplacian $\Delta\mathfrak{u}$):

$$\frac{\mathfrak{u}(x_{i+1}) - 2\mathfrak{u}(x_i) + \mathfrak{u}(x_{i-1})}{h^2} = \mathfrak{u}''_{xx}(x_i) + \frac{h^2}{24}\left(\mathfrak{u}^{(4)}_{xxxx}(\xi_1) + \mathfrak{u}^{(4)}_{xxxx}(\xi_2)\right).$$

Thus, the difference is bounded by the fourth derivative:

$$\left|\frac{\partial^2\mathfrak{u}}{\partial x^2} - \delta_x^2\mathfrak{u}\right| \leq \frac{h^2}{12}\max_{\Omega}\left|\frac{\partial^4\mathfrak{u}}{\partial x^4}\right|. \tag{33}$$

Applying this to both x and y dimensions implies:

$$|E_s| \leq D_{\mathfrak{u}}\frac{h^2}{12}\left(\max\left|\frac{\partial^4\mathfrak{u}}{\partial x^4}\right| + \max\left|\frac{\partial^4\mathfrak{u}}{\partial y^4}\right|\right) = C_s h^2. \tag{34}$$

Combining the temporal and spatial bounds:

$$|R^n_{\mathfrak{u},i,j}| \leq |E_t| + |E_s| \leq C_t(\Delta t)^{2-\alpha} + C_s h^2 \leq C_1\left((\Delta t)^{2-\alpha} + h^2\right).$$

A completely analogous analysis for $\mathfrak{v}$ yields:

$$|R^n_{\mathfrak{v},i,j}| \leq C_2\left((\Delta t)^{2-\alpha} + h^2\right).$$

This completes the proof of the Lemma. □

Theorem 3. *The numerical solution* $(\mathfrak{u}_{i,j}^n, \mathfrak{v}_{i,j}^n)$ *obtained by the fully discrete scheme* (10) *converges to the exact solution* $(\mathfrak{u}(x_i, y_j, t_n), \mathfrak{v}(x_i, y_j, t_n))$ *of the FO RD system. The global error is bounded by:*

$$||\varepsilon^n|| + ||\delta^n|| \leq \tilde{C}((\Delta t)^{2-\alpha} + h^2)$$

where $\tilde{C}$ *is a positive constant independent of the time step* Δt *and grid spacing* h*, provided that the stability condition* $0 < C < 1$ *is satisfied. This implies the scheme is convergent with order* $O((\Delta t)^{2-\alpha} + h^2)$*.*

Proof. The convergence proof relies on the consistency of the scheme and the stability result from Theorem 1. First, we define the truncation errors $R_{\mathfrak{u},i,j}^n$ and $R_{\mathfrak{v},i,j}^n$ by substituting the exact solution $(\mathfrak{u}(x_i, y_j, t_n), \mathfrak{v}(x_i, y_j, t_n))$ into the numerical scheme. Specifically, $R_{\mathfrak{u},i,j}^n$ is the residual obtained when the exact solution is applied to the discretized equation:

$$R_{\mathfrak{u},i,j}^n = L_t^\alpha \mathfrak{u}(x_i, y_j, t_n) - \left[D_\mathfrak{u} \Delta_h \mathfrak{u}(x_i, y_j, t_{n-1}) + f(\mathfrak{u}(x_i, y_j, t_{n-1}), \mathfrak{v}(x_i, y_j, t_{n-1}))\right],$$

where L_t^α denotes the L_1 discrete fractional derivative operator and Δ_h denotes the central difference spatial operator. Explicitly, the L_1 approximation error and the spatial central difference error are given by the Taylor series expansions:

$$L_t^\alpha \mathfrak{u}(x_i, y_j, t_n) = \frac{\partial^\alpha \mathfrak{u}}{\partial t^\alpha}(x_i, y_j, t_n) + C_t (\Delta t)^{2-\alpha} \frac{\partial^2 \mathfrak{u}}{\partial t^2}(\xi_t), \tag{35}$$

$$\Delta_h \mathfrak{u}(x_i, y_j, t_{n-1}) = \Delta \mathfrak{u}(x_i, y_j, t_{n-1}) + \frac{h^2}{12}\left(\frac{\partial^4 \mathfrak{u}}{\partial x^4}(\xi_x) + \frac{\partial^4 \mathfrak{u}}{\partial y^4}(\xi_y)\right). \tag{36}$$

Substituting these expansions into the definition of $R_{\mathfrak{u},i,j}^n$ and utilizing the original differential equation $\frac{\partial^\alpha \mathfrak{u}}{\partial t^\alpha} = D_\mathfrak{u} \Delta \mathfrak{u} + f(\mathfrak{u}, \mathfrak{v})$, we obtain the explicit form of the truncation error:

$$R_{\mathfrak{u},i,j}^n = C_t (\Delta t)^{2-\alpha} \frac{\partial^2 \mathfrak{u}}{\partial t^2}(\xi_t) - \frac{D_\mathfrak{u} h^2}{12}\left(\frac{\partial^4 \mathfrak{u}}{\partial x^4}(\xi_x) + \frac{\partial^4 \mathfrak{u}}{\partial y^4}(\xi_y)\right). \tag{37}$$

Similarly, for the second component $\mathfrak{v}$, the truncation error is given by:

$$R_{\mathfrak{v},i,j}^n = C_t (\Delta t)^{2-\alpha} \frac{\partial^2 \mathfrak{v}}{\partial t^2}(\eta_t) - \frac{D_\mathfrak{v} h^2}{12}\left(\frac{\partial^4 \mathfrak{v}}{\partial x^4}(\eta_x) + \frac{\partial^4 \mathfrak{v}}{\partial y^4}(\eta_y)\right). \tag{38}$$

Taking the absolute value and bounding the higher-order derivatives with constants C_1 and C_2, the total truncation error is bounded by:

$$|R_{\mathfrak{u},i,j}^n| \leq C_1\left((\Delta t)^{2-\alpha} + h^2\right), \quad |R_{\mathfrak{v},i,j}^n| \leq C_2\left((\Delta t)^{2-\alpha} + h^2\right),$$

where C_1 and C_2 are constants depending on the higher-order derivatives of the exact solution. Subtracting the numerical scheme from the exact equations (with truncation error added), we obtain the error evolution equations similar to (24), but with the additional truncation terms:

$$\nabla \varepsilon_{i,j}^n = \mathcal{L}_h(\varepsilon_{i,j}^{n-1}) + \mathcal{N}(\varepsilon, \delta) + R_{\mathfrak{u},i,j}^n, \tag{39}$$

$$\nabla \delta_{i,j}^n = \mathcal{L}_h(\delta_{i,j}^{n-1}) + \mathcal{N}(\varepsilon, \delta) + R_{\mathfrak{v},i,j}^n, \tag{40}$$

where $\mathcal{L}_h$ represents the linear difference operator and $\mathcal{N}$ represents the nonlinear error components. Constructing the energy inequality as done in the stability proof, we multiply by the error terms and sum over the grid. Applying the Cauchy–Schwarz inequality to the new truncation error terms yields:

$$\nabla E^n \leq -CE^{n-1} + 2\sum_{i,j} \left(\varepsilon_{i,j}^n R_{\mathfrak{u},i,j}^n + \delta_{i,j}^n R_{\mathfrak{v},i,j}^n \right). \tag{41}$$

Using Young's inequality ($ab \leq \frac{1}{2}a^2 + \frac{1}{2}b^2$), we bound the cross terms:

$$2\sum_{i,j} \left(\varepsilon_{i,j}^n R_{\mathfrak{u},i,j}^n + \delta_{i,j}^n R_{\mathfrak{v},i,j}^n \right) \leq \|\varepsilon^n\|^2 + \|\delta^n\|^2 + \|R_{\mathfrak{u}}^n\|^2 + \|R_{\mathfrak{v}}^n\|^2. \tag{42}$$

Since the scheme is stable ($0 < C < 1$) and the time step is sufficiently small, the dominant negative feedback from the stability term controls the error growth. Summing the inequalities over time steps $n = 1, \ldots, M$, and noting that the initial error $E^0 = 0$, we find that the total accumulated error is bounded by the sum of the truncation errors:

$$E^{n-1} \leq \frac{1}{1-C} \max_{0 \leq k \leq n} \left(\|R_{\mathfrak{u}}^k\|^2 + \|R_{\mathfrak{v}}^k\|^2 \right). \tag{43}$$

Substituting the bounds for the truncation errors:

$$E^{n-1} \leq \frac{C_1^2 + C_2^2}{1-C} \left((\Delta t)^{2-\alpha} + h^2 \right)^2.$$

Taking the square root of both sides of the inequality, we obtain:

$$\sqrt{E^{n-1}} \leq \sqrt{\frac{C_1^2 + C_2^2}{1-C}} \left((\Delta t)^{2-\alpha} + h^2 \right). \tag{44}$$

Letting $\tilde{C} = \sqrt{\dfrac{(C_1^2 + C_2^2)}{1-C}}$, we have:

$$\|\varepsilon^{n-1}\| + \|\delta^{n-1}\| \leq \tilde{C} \left((\Delta t)^{2-\alpha} + h^2 \right). \tag{45}$$

For $n = 1$, the numerical solution is initialized with the exact initial conditions, so $\varepsilon_{i,j}^0 = 0$ and $\delta_{i,j}^0 = 0$. Consequently, the initial energy is zero:

$$E^0 = \|\varepsilon^0\|^2 + \|\delta^0\|^2 = 0. \tag{46}$$

Thus, the bound holds trivially for the base case. Suppose the stability condition $0 < C < 1$ holds and the time step is sufficiently small. The dominant negative feedback $-CE^{n-1}$ controls the error growth. Using the Cauchy–Schwarz and Young's inequalities on the cross terms $\varepsilon R_{\mathfrak{u}}$ and $\delta R_{\mathfrak{v}}$, and summing the inequalities over time steps $k = 1, \ldots, n$:

$$E^n \leq \frac{1}{1-C} \max_{0 \leq k \leq n+1} \left(\|R_{\mathfrak{u}}^k\|^2 + \|R_{\mathfrak{v}}^k\|^2 \right). \tag{47}$$

Substituting the truncation error bounds from Lemma 1 ($|R| \leq C_i((\Delta t)^{2-\alpha} + h^2)$):

$$E^n \leq \frac{C_1^2 + C_2^2}{1-C} \left((\Delta t)^{2-\alpha} + h^2 \right)^2. \tag{48}$$

Let $\tilde{C} = \sqrt{\frac{C_1^2 + C_2^2}{1-C}}$. Taking the square root of both sides gives the norm of the errors:

$$\|\varepsilon^n\| + \|\delta^n\| \leq \tilde{C} \left((\Delta t)^{2-\alpha} + h^2 \right). \tag{49}$$

Thus, the scheme is convergent with order $O((\Delta t)^{2-\alpha} + h^2)$. □

4 Numerical Application

To demonstrate the efficiency and applicability of the proposed numerical method to real-world biological phenomena, we simulate the classic Brusselator RD model. This model is a theoretical framework often used to describe the formation of dissipative structures and Turing patterns in chemical systems. The simulation is conducted with the following parameter set, which is chosen to satisfy the Turing bifurcation conditions required for spatial instability:

Table 1: Simulation parameters

Category	**Value**
Model Parameters	$\mathfrak{a} = 1$, $\mathfrak{b} = 3$
Diffusion Coefficients	$D_{\mathfrak{u}} = 0.0016$, $D_{\mathfrak{v}} = 0.0131$
Domain Size	$L = 50$
Grid Resolution	$N \times N = 100 \times 100$
Spatial Step Size	$h = \dfrac{L}{N-1}$
Time Step Size	$\Delta t = 0.1$

The numerical solution is computed over the two-dimensional square domain $\Omega = [0, L] \times [0, L]$. The spatial Laplacian operators are approximated using the standard five-point central difference stencil with truncation error of order $O(h^2)$, while the time-fractional derivative is handled using the proposed discrete scheme. To ensure the system remains closed, we impose homogeneous Neumann (zero-flux) boundary conditions at the domain edges:

$$\nabla \mathfrak{u} \cdot \mathbf{n} = 0, \quad \nabla \mathfrak{v} \cdot \mathbf{n} = 0, \quad \text{on } \partial\Omega, \tag{50}$$

where $\mathbf{n}$ is the outward normal vector.

The Turing instability is triggered by perturbing the homogeneous steady state $(\mathfrak{u}^*, \mathfrak{v}^*) = (\mathfrak{a}, \mathfrak{b}/\mathfrak{a}) = (1, 3)$. The initial conditions are set as:

$$\mathfrak{u}(x, y, 0) = \mathfrak{u}^* + \delta_{rnd}, \quad \mathfrak{v}(x, y, 0) = \mathfrak{v}^* + \delta_{rnd}, \tag{51}$$

where δ_{rnd} represents small random Gaussian noise with an amplitude of 10^{-4}, simulating natural fluctuations in the chemical concentrations. The iterative process is executed until the system reaches a stable spatiotemporal pattern.

The numerical procedure adopted for the simulation is outlined in Algorithm 1.

Algorithm 1 Numerical Simulation of the Brusselator Model

Input: Parameters $\mathfrak{a}, \mathfrak{b}, D_\mathfrak{u}, D_\mathfrak{v}, L, N, \Delta t, T_{max}$
Initialize Grid:
  Calculate spatial step $h = L/(N-1)$
  Define steady state: $\mathfrak{u}^* = \mathfrak{a}$, $\mathfrak{v}^* = \mathfrak{b}/\mathfrak{a}$
  Initialize fields: $\mathfrak{u}_{i,j} = \mathfrak{u}^* + \text{noise}$, $\mathfrak{v}_{i,j} = \mathfrak{v}^* + \text{noise}$
Time Stepping:
for $n = 1$ to $T_{max}/\Delta t$ **do**
    Compute Laplacians (using 5-point stencil):
      Apply Neumann Boundary Conditions (mirror neighbors)
      $\mathcal{L}\mathfrak{u}_{i,j} \leftarrow \frac{\mathfrak{u}_{i+1,j}+\mathfrak{u}_{i-1,j}+\mathfrak{u}_{i,j+1}+\mathfrak{u}_{i,j-1}-4\mathfrak{u}_{i,j}}{h^2}$
      $\mathcal{L}\mathfrak{v}_{i,j} \leftarrow \frac{\mathfrak{v}_{i+1,j}+\mathfrak{v}_{i-1,j}+\mathfrak{v}_{i,j+1}+\mathfrak{v}_{i,j-1}-4\mathfrak{v}_{i,j}}{h^2}$
    Compute Reaction Terms:
      $f(\mathfrak{u}, \mathfrak{v}) \leftarrow \mathfrak{a} - (\mathfrak{b}+1)\mathfrak{u}_{i,j} + \mathfrak{u}_{i,j}^2\mathfrak{v}_{i,j}$
      $g(\mathfrak{u}, \mathfrak{v}) \leftarrow \mathfrak{b}\mathfrak{u}_{i,j} - \mathfrak{u}_{i,j}^2\mathfrak{v}_{i,j}$
    Update Solution:
      $\mathfrak{u}_{i,j}^{new} \leftarrow \mathfrak{u}_{i,j} + \Delta t(D_\mathfrak{u}\mathcal{L}\mathfrak{u}_{i,j} + f(\mathfrak{u}, \mathfrak{v}))$
      $\mathfrak{v}_{i,j}^{new} \leftarrow \mathfrak{v}_{i,j} + \Delta t(D_\mathfrak{v}\mathcal{L}\mathfrak{v}_{i,j} + g(\mathfrak{u}, \mathfrak{v}))$
    Update Time: $t \leftarrow t + \Delta t$
end for
Output: Spatial distribution of $\mathfrak{u}$ and $\mathfrak{v}$

The simulation results depicting the evolution of the activator species $\mathfrak{u}$ are presented in Figure 2. Initially, the system exhibits small random fluctuations around the equilibrium point. As the simulation progresses, the diffusion-driven instability mechanism acts to amplify specific spatial modes. Due to the significant difference in diffusion coefficients ($D_{\mathfrak{v}} \gg D_{\mathfrak{u}}$) and the autocatalytic nature of $\mathfrak{u}$, the symmetry of the homogeneous state is broken. The proposed numerical scheme, with its theoretical convergence order of $O((\Delta t)^{2-\alpha} + h^2)$, effectively captures the transition from thermodynamic equilibrium to a self-organized state. As shown in Figure 2, the system eventually settles into a stable stationary Turing pattern. The formation of these dissipative structures confirms that the numerical method preserves the positivity and stability properties of the continuous model, effectively reproducing the complex nonlinear dynamics predicted by the theoretical analysis.

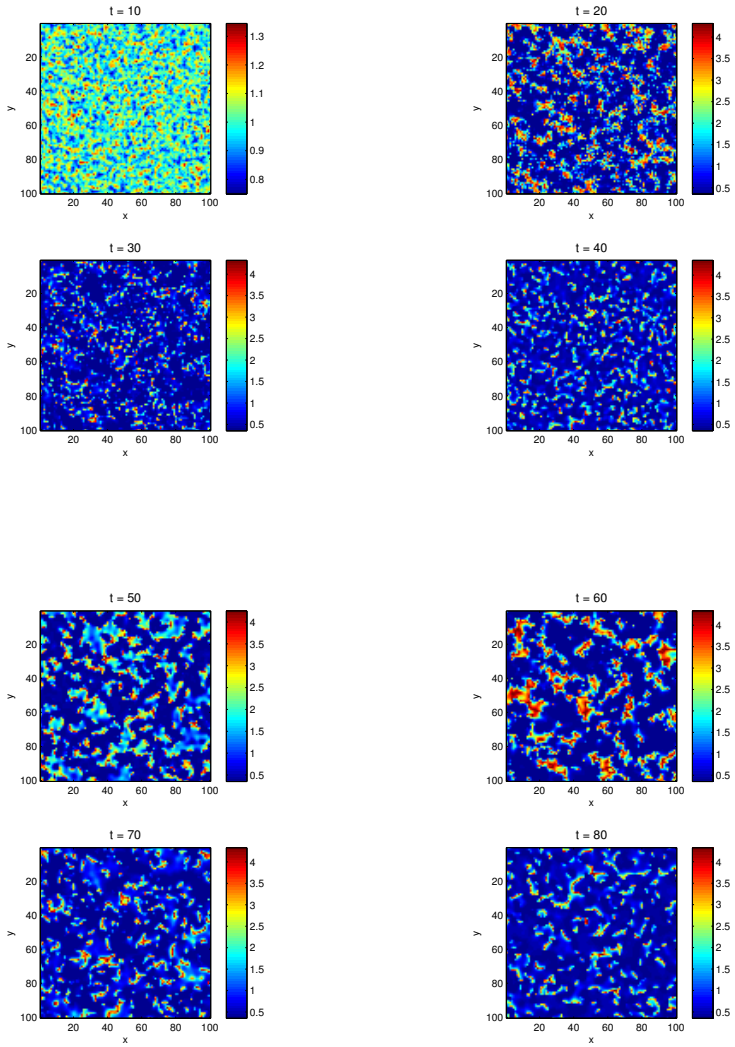

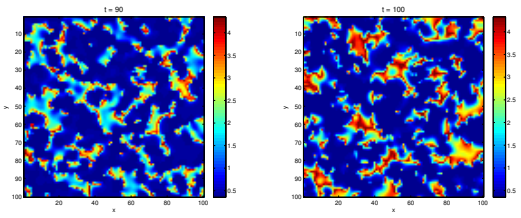

Figure 1: Formation of stationary, self-organized spatial Turing patterns for the concentration component u under fractional diffusion.

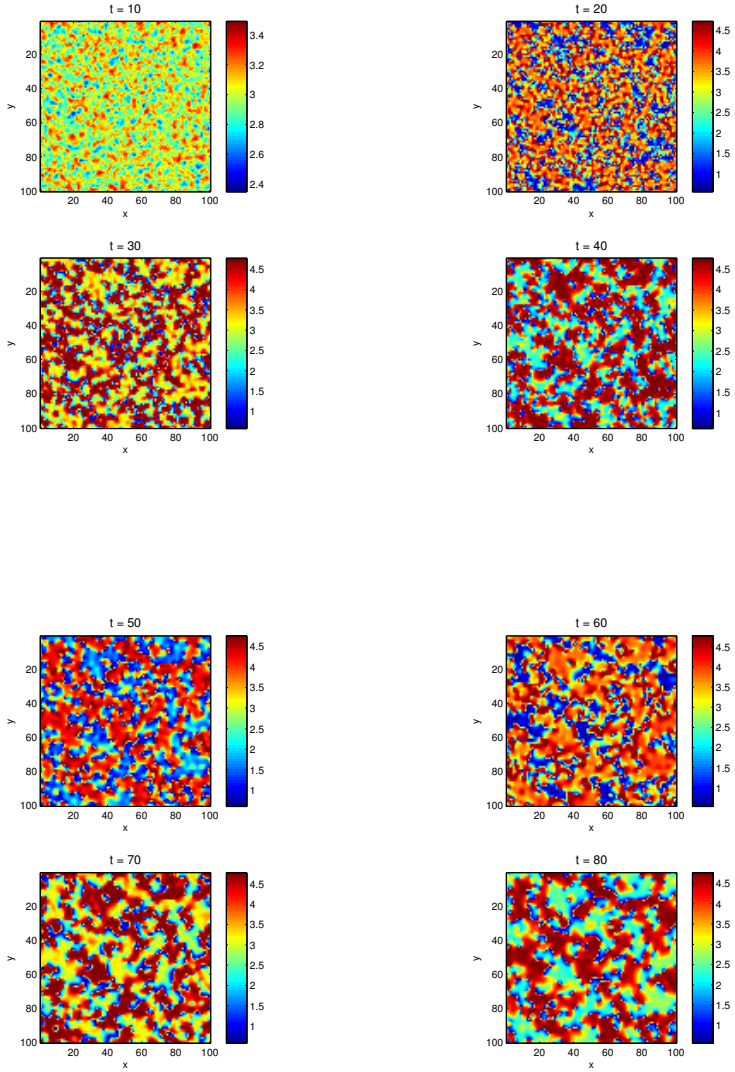

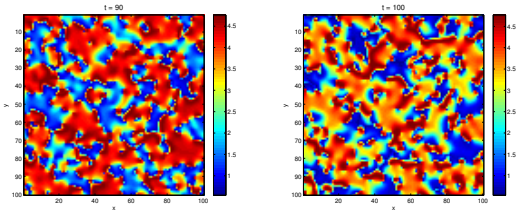

Figure 2: Formation of stationary, self-organized spatial Turing patterns for the concentration component v under fractional diffusion.

5 Conclusion

In this paper, we have investigated the FO RD Brusselator model as a theoretical framework for studying the emergence of spatiotemporal patterns in systems far from equilibrium. By extending the classical Brusselator with Caputo fractional time derivatives, we have introduced a more flexible modeling tool capable of capturing memory effects and anomalous diffusion phenomena often observed in complex biological and chemical systems. A fully discrete numerical scheme based on the L_1 approximation for the time-fractional derivative and a five-point FDM for the spatial Laplacian has been developed. The proposed method is proven to be well-posed, asymptotically stable, and convergent with an order of $O((\Delta t)^{2-\alpha} + h^2)$, under a mild condition on the discretization parameters. Theoretical guarantees regarding the uniqueness of the numerical solution (Theorem 1), its stability (Theorem 2), and its convergence to the exact solution (Theorem 3) have been rigorously established.

Numerical simulations of the FO Brusselator model under Turing-unstable conditions successfully reproduce the formation of stationary, self-organized spatial patterns, confirming the ability of the scheme to capture the essential nonlinear dynamics of the system. The results illustrate how the interplay between fractional time evolution, differential diffusion, and nonlinear kinetics can lead to symmetry breaking and pattern formation, consistent with the classical Turing mechanism. The methodology presented here provides a reliable computational tool for exploring FO-RD systems in two dimensions. Future work may involve extending the approach to three-dimensional domains, considering other types of fractional operators, or applying the model to specific biological contexts such as morphogenesis, skin pigmentation, or neural field dynamics. The theoretical and numerical framework established in this study offers a solid foundation for further investigations into the role of fractional calculus in pattern-forming systems.

References

[1] M. J. Thompson, H. G. Othmer, and D. M. Umulis, "A primer on reaction–diffusion models in embryonic development," *Encyclopedia of Life Sciences*, pp. 1–16, 2018.

[2] S. Kondo and T. Miura, "Reaction-diffusion model as a framework for understanding biological pattern formation," *Science*, vol. 329, no. 5999, pp. 1616–1620, 2010.

[3] J. Tabony, "Historical and conceptual background of self-organization by reactive processes," *Biology of the Cell*, vol. 98, no. 10, pp. 589–602, 2006.

[4] A. N. Landge, B. M. Jordan, X. Diego, and P. Müller, "Pattern formation mechanisms of self-organizing reaction-diffusion systems," *Developmental Biology*, vol. 460, no. 1, pp. 2–11, 2020.

[5] C. Curantz and M. Manceau, "Trends and variation in vertebrate patterns as outcomes of self-organization," *Current Opinion in Genetics & Development*, vol. 69, pp. 147–153, 2021.

[6] J. D. Rolston, D. A. Wagenaar, and S. M. Potter, "Precisely timed spatiotemporal patterns of neural activity in dissociated cortical cultures," *Neuroscience*, vol. 148, no. 1, pp. 294–303, 2007.

[7] A. Chatterjee, N. Mears, Y. Yadati, and G. S. Iannacchione, "An overview of emergent order in far-from-equilibrium driven systems: From Kuramoto oscillators to Rayleigh–Bénard convection," *Entropy*, vol. 22, no. 5, p. 561, 2020.

[8] O. Descalzi, M. Clerc, S. Residori, and G. Assanto, Eds., *Localized States in Physics: Solitons and Patterns*. New York, NY, USA: Springer, 2011.

[9] R. A. Satnoianu, M. Menzinger, and P. K. Maini, "Turing instabilities in general systems," *Journal of Mathematical Biology*, vol. 41, no. 6, pp. 493–512, 2000.

[10] R. A. Barrio, "Turing systems: A general model for complex patterns in nature," in *Physics of Emergence and Organization*, Berlin, Germany: Springer, 2008, pp. 267–296.

[11] B. I. Henry and S. L. Wearne, "Existence of Turing instabilities in a two-species fractional reaction–diffusion system," *SIAM Journal on Applied Mathematics*, vol. 62, no. 3, pp. 870–887, 2002.

[12] R. A. Satnoianu, M. Menzinger, and P. K. Maini, "Turing instabilities in general systems," *Journal of Mathematical Biology*, vol. 41, no. 6, pp. 493–512, 2000.

[13] M. E. Hohn, B. Li, and W. Yang, "Analysis of coupled reaction–diffusion equations for RNA interactions," *Journal of Mathematical Analysis and Applications*, vol. 425, no. 1, pp. 212–233, 2015.

[14] I. Prigogine and G. Nicolis, "On symmetry-breaking instabilities in dissipative systems," *The Journal of Chemical Physics*, vol. 46, no. 9, pp. 3542–3550, 1967.

[15] B. De Dier and D. Roose, "Determination of bifurcation points and catastrophes for the Brusselator model with two parameters," in *Bifurcation: Analysis, Algorithms, Applications*, Basel, Switzerland: Birkhäuser, 1987.

[16] L. Diambra, V. R. Senthivel, D. B. Menendez, and M. Isalan, "Cooperativity to increase Turing pattern space for synthetic biology," *ACS Synthetic Biology*, vol. 4, no. 2, pp. 177–186, 2015.

[17] K. Wang, M. L. Steyn-Ross, D. A. Steyn-Ross, M. T. Wilson, J. W. Sleigh, and Y. Shiraishi, "Simulations of pattern dynamics for reaction-diffusion systems via SIMULINK," *BMC Systems Biology*, vol. 8, no. 1, p. 45, 2014.

[18] Anber, A.N., Dahmani, Z.: The Laplace Decomposition Method for Solving Nonlinear Conformable Fractional Evolution Equations. Int. J. Open Problems Compt. Math. **17**(1), 67–81 (2024)

[19] A. De Wit, D. Lima, G. Dewel, and P. Borckmans, "Spatiotemporal dynamics near a codimension-two point," *Physical Review E*, vol. 54, no. 1, pp. 261–271, 1996.

[20] S. Vaidyanathan, "Dynamics and control of Brusselator chemical reaction," *International Journal of ChemTech Research*, vol. 8, no. 6, pp. 740–749, 2015.

[21] I. H. Jebril and I. Batiha, "A stable and convergent implicit finite difference scheme for variable-order time-fractional convection–diffusion equations," *Int. J. Open Problems Compt. Math.*, vol. 19, no. 1, pp. 73–94, 2026.

[22] D. J. Needham and J. Billingham, "The non-local Lotka–Volterra system with a top hat kernel—Part 1: Dynamics and steady states with small diffusivity," *Proceedings of the Royal Society A*, vol. 479, no. 2277, p. 20230381, 2023.

[23] Berir, M.: Analysis of the Effect of White Noise on the Halvorsen System of Variable-Order Fractional Derivatives Using a Novel Numerical Method. Int. J. Adv. Soft Comput. Appl. **16**(3), 294–306 (2024).

[24] T. Drengstig, X. Y. Ni, K. Thorsen, I. W. Jolma, and P. Ruoff, "Robust adaptation and homeostasis by autocatalysis," *The Journal of Physical Chemistry B*, vol. 116, no. 18, pp. 5355–5363, 2012.

[25] Singh, P., Zade, N., Priyadarshi, P., Gupte, A.: The Application of Machine Learning and Deep Learning Techniques for Global Energy Utilization Projection for Ecologically Responsible Energy Management. Int. J. Adv. Soft Comput. Appl. **17**(1), 49–66 (2025).

[26] W. Duch and K. Dobosz, "Visualization for understanding of neurodynamical systems," *Cognitive Neurodynamics*, vol. 5, no. 2, pp. 145–160, 2011.

[27] Mohammed, E. A., Lakizadeh, A.: Benchmarking Vision Transformers for Satellite Image Classification based on Data Augmentation Techniques. Int. J. Adv. Soft Comput. Appl. **17**(1), 98–114 (2025).

[28] J. L. Suzuki, M. Gulian, M. Zayernouri, and M. D'Elia, "Fractional modeling in action: A survey of nonlocal models for subsurface transport, turbulent flows, and anomalous materials," *Journal of Peridynamics and Nonlocal Modeling*, vol. 5, no. 3, pp. 392–459, 2023.

[29] A. Anber and Z. Dahmani, "Solutions of the reaction-diffusion Brusselator with fractional derivatives," *Journal of Interdisciplinary Mathematics*, vol. 17, no. 5–6, pp. 451–460, 2014.

[30] M. Amirian Matlob and Y. Jamali, "The concepts and applications of fractional order differential calculus in modelling of viscoelastic systems: A primer," arXiv:1706.xxxxx, 2017.

[31] S. Srivastava and K. Garikipati, "Pattern formation in dense populations studied by inference of nonlinear diffusion–reaction mechanisms," *International Journal for Numerical Methods in Engineering*, vol. 125, no. 12, p. e7475, 2024.

[32] W. E. Schiesser and G. W. Griffiths, *A Compendium of Partial Differential Equation Models: Method of Lines Analysis with MATLAB*. Cambridge, U.K.: Cambridge Univ. Press, 2009.

[33] G. W. Recktenwald, "Finite-difference approximations to the heat equation," *Mechanical Engineering*, vol. 10, no. 1, 2004.

[34] R. J. LeVeque, "Semi-discrete methods," in *Numerical Methods for Conservation Laws*. Basel, Switzerland: Birkhäuser, 1992, pp. 193–199.

[35] A. Ern and J.-L. Guermond, "Semi-discretization in space," in *Finite Elements III: First-Order and Time-Dependent PDEs*. Cham, Switzerland: Springer, 2021, pp. 135–146.

[36] A. Padder, L. Almutairi, S. Qureshi, A. Soomro, A. Afroz, E. Hincal, and A. Tassaddiq, "Dynamical analysis of generalized tumor model with Caputo fractional-order derivative," *Fractal and Fractional*, vol. 7, no. 3, p. 258, 2023.

[37] K. Abuasbeh, A. Kanwal, R. Shafqat, B. Taufeeq, M. A. Almulla, and M. Awadalla, "A method for solving time-fractional initial boundary value problems of variable order," *Symmetry*, vol. 15, no. 2, p. 519, 2023.

[38] T. Hytönen, J. van Neerven, M. Veraar, and L. Weis, *Analysis in Banach Spaces*. Berlin, Germany: Springer, 2016.